

# Non-Reciprocal Antenna Array Based on Magnetized Graphene for THz Applications Using the Iterative Method

Aymen Hlali\*, Zied Houaneb, and Hassen Zairi

**Abstract**—An effective and precise approach to the Wave Concept Iterative Process method modeling of magnetized graphene sheet as an anisotropic conductive surface is used to analyze the anisotropy of magnetostatically biased graphene and for studying an electrically doped magnetically biased graphene non-reciprocal antenna array for THz applications. The tuning of the performance of the array antenna is possible by varying the magnetic field and the chemical potential of graphene material. The return loss value decreases by increasing the magnetostatic bias and increases when the chemical potential increases.

## 1. INTRODUCTION

Non-reciprocal components are ubiquitous in electronic and optical systems. According to recent progress in graphene research, it has been shown that graphene exhibits gyrotropic properties, making it a promising candidate for the realization of non-reciprocal devices [1–4]. Furthermore, the combined application of magnetic bias and electrical doping in graphene can be leveraged towards tunable and versatile non-reciprocal plasmonic components. Several groups have proposed non-reciprocal components based on graphene's such as antennas, couplers, circulators, phase shifters, and other non-reciprocal devices [5–10].

Along with this research process, new methods are much in demand to model-based electronic devices based on the magnetized graphene [10–15]. In most of the numerical methods, magnetized graphene is usually incorporated in the algorithm by transforming the surface conductivity to a volumetric conductivity by dividing the thickness of the graphene, which might introduce a multiscale computational problem in simulation, require massive CPU time and memory, and make the optimization process tiresome. In order to overcome this problem, the wave concept iterative process method can be applied by treating the 2D materials as conductive surface boundaries, to not only yield precision in the result, but also reduce the time consumption and memory size [16–25].

In summary, we investigate a reconfigurable and non-reciprocal antenna array based on magnetized graphene over an ultrawide terahertz band using the Wave Concept Iterative Process method. In particular, the response of the proposed array antenna can be controlled conveniently by adjusting the chemical potential and the magnetic field of graphene. The remaining part of this paper is organized as follows. In Section 2, some theoretical aspects about the anisotropic surface conductivity of graphene and a brief overview to the WCIP method are described. Section 3 investigates numerical results to demonstrate the capability of the proposed algorithm for the modeling and simulation of non-reciprocal antenna array for THz applications. Some conclusions are presented in Section 4.

---

*Received 22 November 2019, Accepted 16 January 2020, Scheduled 30 January 2020*

\* Corresponding author: Aymen Hlali (Hlaliaymen683@gmail.com).

The authors are with the Research Laboratory Smart Electricity & ICT, SEICT, National Engineering School of Carthage, University of Carthage, Tunis, Tunisia.

## 2. THEORY AND FORMULATION

### 2.1. Conductivity Model of Magnetized Graphene

The magnetized graphene is an infinitesimally thin sheet biased by a magnetostatic field and behaves as an anisotropic conducting sheet characterized by a conductivity tensor [26–29]

$$\bar{\sigma} = \begin{pmatrix} \sigma_d & -\sigma_o \\ \sigma_o & \sigma_d \end{pmatrix} \quad (1)$$

The expressions of  $\sigma_d$  and  $\sigma_o$  can be approximated by a Drude-like model [14, 28], which are

$$\sigma_d = \sigma \frac{1 + j\omega\tau}{(\omega_c\tau)^2 + (1 + j\omega\tau)^2} \quad (2)$$

$$\sigma_o = \sigma \frac{\omega_c\tau}{(\omega_c\tau)^2 + (1 + j\omega\tau)^2} \quad (3)$$

with

$$\sigma = \frac{e^2\tau K_B T}{\pi\hbar^2} \left[ \frac{\mu_c}{K_B T} + 2 \ln \left( e^{-\frac{\mu_c}{K_B T}} + 1 \right) \right] \quad (4)$$

where  $\tau$  is the phenomenological scattering time,  $\omega_c = \frac{eBv_F^2}{\mu_c}$  the cyclotron frequency,  $B$  the amplitude of the static magnetic field bias,  $e$  the electron charge,  $K_B$  the Boltzmann constant,  $T$  the room temperature,  $v_F$  the Fermi velocity,  $\mu_c$  the chemical potential, and  $\hbar$  the reduced Plancks constant.

### 2.2. Formulation of WCIP Method

The classic WCIP method has been described in detail in various articles [16–25]. This method is presented by writing the electric field and current density in terms of waves. We can express these combinations by the following equations

$$\vec{A}_i = \frac{1}{2\sqrt{Z_{0i}}} (\vec{E}_i + Z_{0i}\vec{J}_i) \quad i = 1, 2 \quad (5)$$

$$\vec{B}_i = \frac{1}{2\sqrt{Z_{0i}}} (\vec{E}_i - Z_{0i}\vec{J}_i) \quad i = 1, 2 \quad (6)$$

where  $\vec{A}_i$  and  $\vec{B}_i$  are, respectively, the incident and the reflected waves.  $Z_{0i}$  is the characteristic impedance of the middle  $i$  ( $i = 1, 2$ ) given by  $Z_{0i} = \sqrt{\frac{\mu_0}{\varepsilon_0\varepsilon_{ri}}}$  where  $\varepsilon_{ri}$  is the relative permittivity of the region  $i$ .  $\vec{J}_i$  is the surface tangential current density which define  $\vec{J}_i = \vec{H}_i \times \vec{n}_i$ .

### 2.3. Formulation of the Magnetized Graphene in WCIP Method

The implementation of the boundary conditions of the magnetized graphene in the WCIP method has been demonstrated in detail in this article [25]. After some manipulation, we can derive the scattering matrix of the magnetized graphene as

$$\begin{pmatrix} \vec{B}_{1,x} \\ \vec{B}_{1,y} \\ \vec{B}_{2,x} \\ \vec{B}_{2,y} \end{pmatrix} = \underbrace{\begin{pmatrix} S_{11}^{Gm} & S_{12}^{Gm} & S_{13}^{Gm} & S_{14}^{Gm} \\ S_{21}^{Gm} & S_{22}^{Gm} & S_{23}^{Gm} & S_{24}^{Gm} \\ S_{31}^{Gm} & S_{32}^{Gm} & S_{33}^{Gm} & S_{34}^{Gm} \\ S_{41}^{Gm} & S_{42}^{Gm} & S_{43}^{Gm} & S_{44}^{Gm} \end{pmatrix}}_{\Gamma_{Gm}} \begin{pmatrix} \vec{A}_{1,x} \\ \vec{A}_{1,y} \\ \vec{A}_{2,x} \\ \vec{A}_{2,y} \end{pmatrix}$$

where  $S_{ij}^{Gm}$  are defined by

$$S_{11}^{Gm} = \frac{X_4 X_1 - X_2^2}{X_1^2 + X_2^2}; \quad S_{12}^{Gm} = \frac{X_4 X_2}{X_1^2 + X_2^2}$$

$$\begin{aligned}
S_{13}^{Gm} &= \frac{2X_1(Z_{02}\sqrt{Z_{01}})}{X_1^2 + X_2^2}; & S_{14}^{Gm} &= \frac{2\sigma_o\sqrt{Z_{01}}(Z_{02}\sqrt{Z_{01}})^2}{X_1^2 + X_2^2} \\
S_{21}^{Gm} &= \frac{-2\sigma_o(Z_{02}\sqrt{Z_{01}})^2}{X_1^2 + X_2^2}; & S_{22}^{Gm} &= S_{11}^{Gm}; & S_{31}^{Gm} &= \frac{2X_1(Z_{01}\sqrt{Z_{02}})}{\sqrt{Z_{01}}[X_1^2 + X_3^2]} \\
S_{23}^{Gm} &= \frac{-2\sigma_o(Z_{02}\sqrt{Z_{01}})^2}{\sqrt{Z_{02}}[X_1^2 + X_2^2]}; & S_{24}^{Gm} &= \frac{2X_1(Z_{02}\sqrt{Z_{01}})}{\sqrt{Z_{02}}[X_1^2 + X_2^2]} \\
S_{32}^{Gm} &= \frac{2\sigma_o(Z_{01}\sqrt{Z_{02}})^2}{X_1^2 + X_3^2}; & S_{33}^{Gm} &= \frac{X_5X_1 - X_3^2}{X_1^2 + X_3^2}; & S_{34}^{Gm} &= S_{32}^{Gm} \\
S_{41}^{Gm} &= \frac{-2\sigma_o\sqrt{Z_{02}}(Z_{01}\sqrt{Z_{02}})^2}{\sqrt{Z_{01}}(X_1^2 - X_3^2)}; & S_{42}^{Gm} &= \frac{2X_1(Z_{01}\sqrt{Z_{02}})}{\sqrt{Z_{01}}(X_1^2 - X_3^2)} \\
S_{43}^{Gm} &= \frac{-2\sigma_o(Z_{01}\sqrt{Z_{02}})^2}{X_1^2 - X_3^2}; & S_{44}^{Gm} &= \frac{X_5X_1 - X_3^2}{X_1^2 - X_3^2}
\end{aligned}$$

and

$$X_1 = Z_{02} + Z_{01} + \sigma_d Z_{01} Z_{02} \quad (7)$$

$$X_2 = (\sigma_o\sqrt{Z_{01}})(Z_{02}\sqrt{Z_{01}}) \quad (8)$$

$$X_3 = (\sigma_o\sqrt{Z_{02}})(Z_{01}\sqrt{Z_{02}}) \quad (9)$$

$$X_4 = Z_{02} - Z_{01} - \sigma_d Z_{01} Z_{02} \quad (10)$$

$$X_5 = Z_{01} - Z_{02} - \sigma_d Z_{01} Z_{02} \quad (11)$$

### 3. NUMERICAL RESULTS AND DISCUSSION

According to the conductivity, there are different scenarios for the properties of the material. The usual case is obtained when the properties are not dependent on the direction; this is the case of the isotropic graphene. Contrary to the case of isotropic surfaces, the anisotropic case occurs when the parts of the conductivity components are different  $\text{Im}_{(\sigma_d)} \neq \text{Im}_{(\sigma_o)}$  and  $\text{Re}_{(\sigma_d)} \neq \text{Re}_{(\sigma_o)}$ . Fig. 1 illustrates the surface conductivity  $\sigma_d$  and  $\sigma_o$  of a graphene sheet. The variation of the graphene conductivity versus the biasing magnetostatic fields  $B$  and the chemical potential  $\mu_c$  is simulated at 2 THz.

Obtained results prove a high anisotropy of the conductivity components. It is clear from these figures that two parameters can control conductivity: the magnetic field  $B$  and the chemical potential  $\mu_c$ . Note that in conventional gyrotropic material, such as ferrites, the constitutive parameters depend only on the magnetic field. In graphene, the chemical potential  $\mu_c$  can be controlled via an electrostatic potential. Fig. 1(d) presents the relationship between bias voltage and chemical potential for an Arlon substrate with thickness 3  $\mu\text{m}$ .

Next, in order to demonstrate the accuracy of the proposed algorithm for modeling of non-reciprocal devices, a program in FORTRAN has been written to simulate a non-reciprocal antenna array for THz applications. The array antenna is placed in the  $xy$ -plane and biased by a magnetic field,  $B$ , in the  $z$ -axis direction. As shown in Fig. 2, an antenna array is printed on an Arlon substrate with dielectric constant of  $\epsilon_r = 3$  which is typically illuminated by an  $x$ -polarized plane wave. The length and width of the substrate are kept fixed at 100  $\mu\text{m}$  and 60  $\mu\text{m}$ , respectively, whereas the height is 3  $\mu\text{m}$ . The gray area represents the graphene, and the white area describes the dielectric substrate.

In order to examine the results obtained by the WCIP method, we begin by studying the boundary conditions. Fig. 3 shows the variation of the reflection coefficient as a function of the number of iterations at the resonant frequency. We find that the convergence is obtained from 300 iterations.

Figures 4(a) and 4(b) illustrate the current density distribution  $|J_x|$  and the electric field distribution  $|E_x|$  of the proposed structure. According to these figures, we notice that the electric field and current density satisfy the boundary conditions, since the density of the current is defined only on the graphene, and zero on the dielectric. The electric field is zero on graphene, and different from zero on the dielectric.

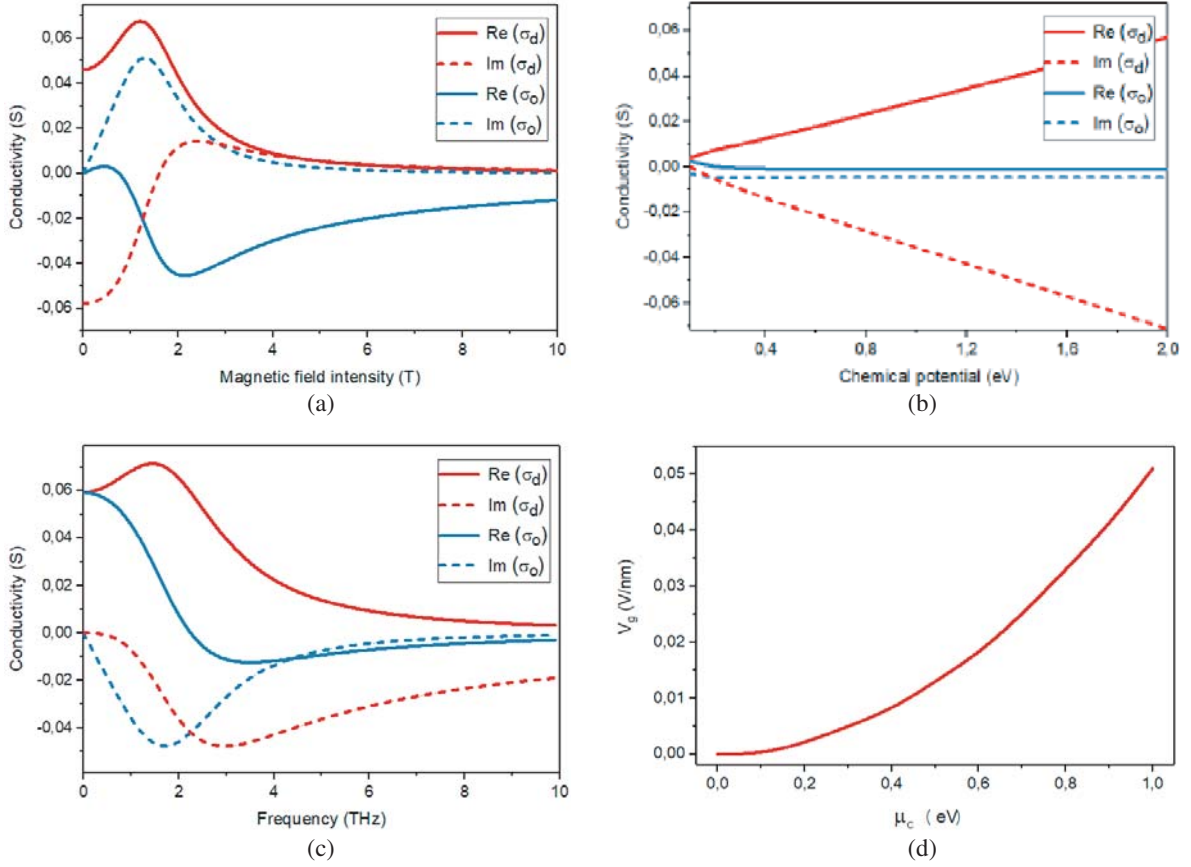


**Figure 1.** Variation of graphene conductivity versus: (a) Biasing magnetostatic fields  $B$ , (b) chemical potential  $\mu_c$ , (c) frequency, and (d) relationship between bias voltage and chemical potential. Graphene parameters are selected as  $\tau = 0.1$  ps,  $T = 300$  K.

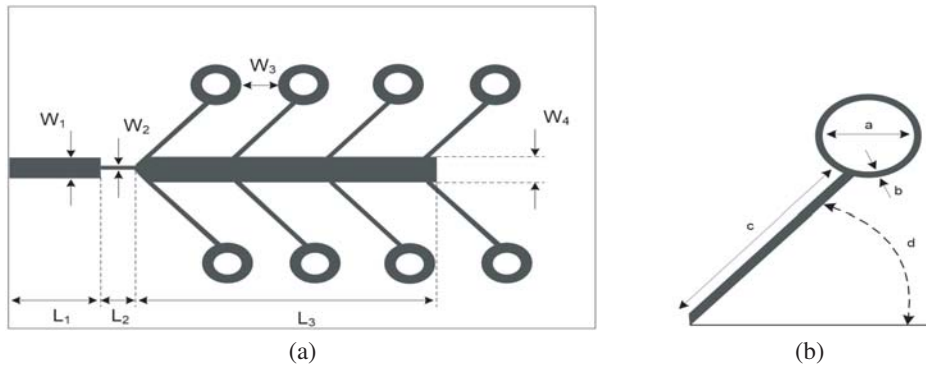


**Figure 2.** Schematic of the proposed array antenna: (a) Top view, and (b) geometric parameters of the radiation patch. Parameters are  $W_1 = 12.8 \mu\text{m}$ ,  $W_2 = 4.26 \mu\text{m}$ ,  $W_3 = 10.24 \mu\text{m}$ ,  $W_4 = 21.33 \mu\text{m}$ ,  $L_1 = 28.16 \mu\text{m}$ ,  $L_2 = 8.96 \mu\text{m}$ ,  $L_3 = 87.04 \mu\text{m}$ ,  $a = 10.24 \mu\text{m}$ ,  $b = 2.56 \mu\text{m}$ ,  $c = 28.16 \mu\text{m}$ ,  $d = 45^\circ$ .

Further, we study the influences of graphene parameters on the antenna array performances. Fig. 5 shows the simulation results obtained under the chemical potential of 0.5 eV with different magnetostatic bias.

Figure 5(b) shows the tunability of the resonance frequency  $f_r$  and the bandwidth  $\Delta f_r$  with changing the magnetostatic bias. It is seen that as  $B$  increases from 1 to 6 T, the value of  $f_r$  is

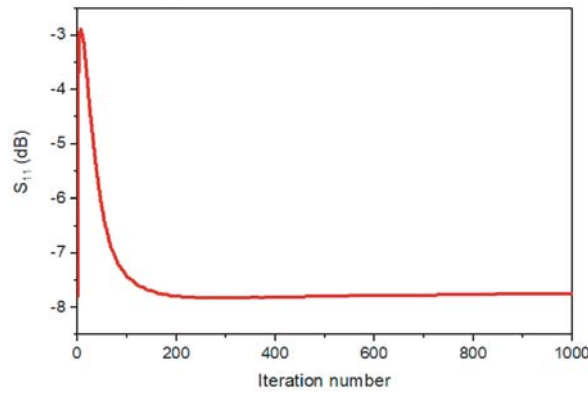


**Figure 3.** Convergence of the reflection coefficient  $S_{11}$  versus number of iterations.

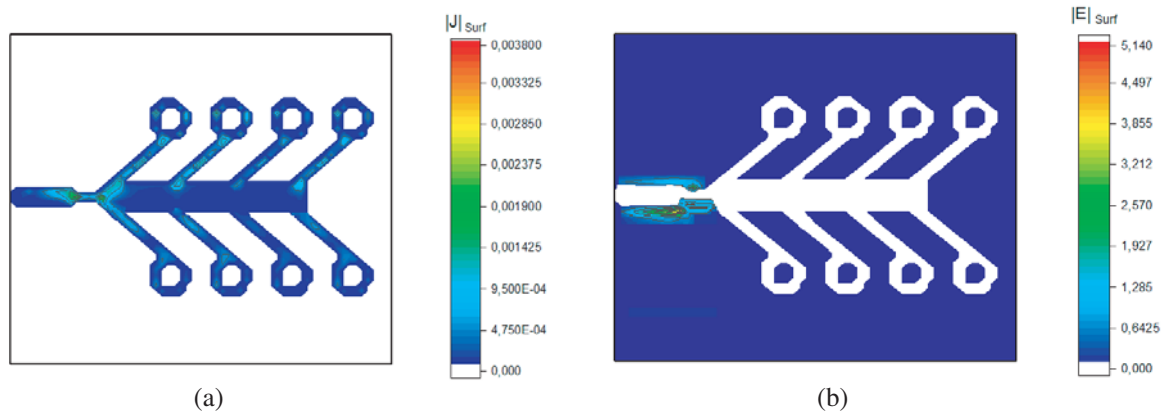


**Figure 4.** (a) Distribution of the current density of the interface  $|J_x|$ , and (b) distribution of the electric field of the interface  $|E_x|$ .

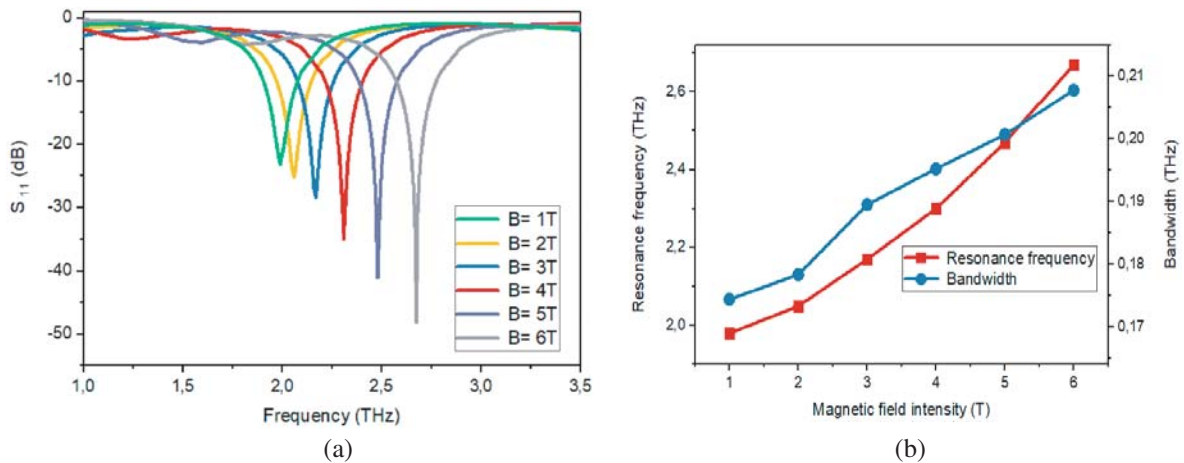


**Figure 5.** (a) Simulated results for different magnetic fields, and (b) variation of resonance frequency and bandwidth.

increased from 1.98 to 2.67 THz, and  $\Delta f_r$  is varied from 0.173 to 0.203 THz. It can be seen that the return loss value decreases by increasing the magnetostatic bias.

The simulation results obtained of this antenna array under different chemical potentials while

the magnetostatic bias is 1 T are shown in Fig. 6. It can be seen from Fig. 6(b) that the maximum value increases when the chemical potential increases, and the resonant frequency shifts toward high frequencies with higher amplitude.

The  $E$  and  $H$ -planes radiation patterns properties of the antenna array are shown in Fig. 7. The results show that the parameters of graphene have significant impacts on the magnitude of the lobe in the  $E$ -plane and  $H$ -plane, in which the radiation pattern becomes more directive by increasing the magnetic field and chemical potential.

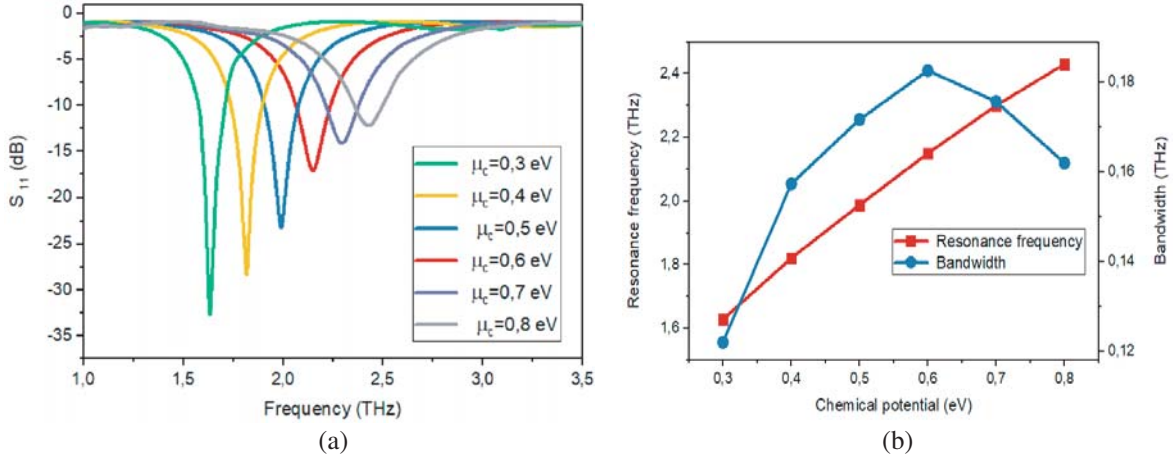


**Figure 6.** (a) Simulated results for different chemical potentials, and (b) variation of resonance frequency and bandwidth.

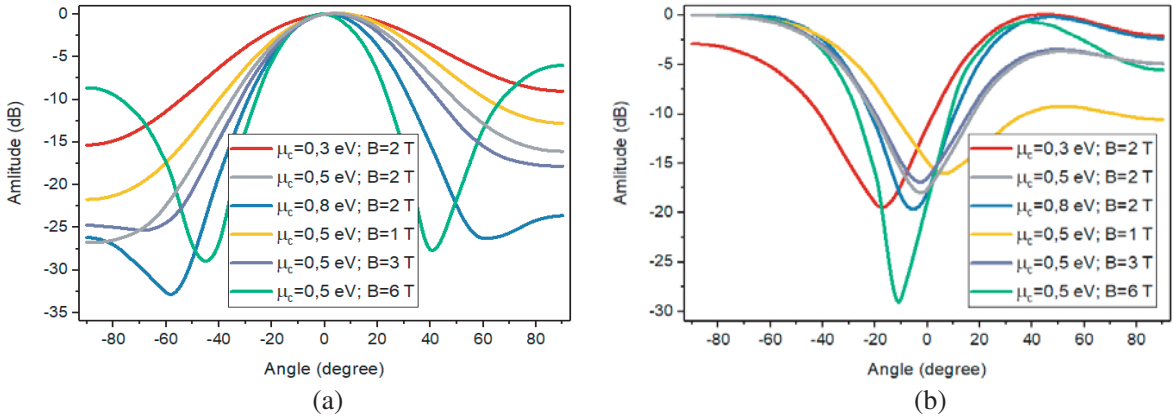


**Figure 7.** (a) Radiation pattern in the  $E$ -plane, and (b) radiation pattern in the  $H$ -plane.

#### 4. CONCLUSION

In conclusion, we have theoretically demonstrated how the magnetized graphene can serve a reconfigurable and non-reciprocal antenna array at THz frequencies using the iterative method, whose properties have been investigated versus the parameters of graphene. In addition, the proposed non-reciprocal array antenna is fully planar, compatible with integrated and optoelectronic circuits, and inherently reconfigurable. The proposed strategy of magnetized graphene could be used to build 2D anisotropic plasmonic devices with enhanced functionalities at THz band and important applications in imaging and communications.

## REFERENCES

1. Crassee, I., J. Levallois, A. L. Walter, M. Ostler, A. Bostwick, E. Rotenberg, T. Seyller, D. D. Marel, A. B. Kuzmenko, "Giant Faraday rotation in single- and multilayer graphene," *Nature Physics*, Vol. 7, 48–51, 2011.
2. Sounas, D. L. and C. Caloz, "Electromagnetic nonreciprocity and gyrotropy of graphene," *Applied Physics Letters*, Vol. 98, 021911, 2011.
3. Sounas, D. L. and C. Caloz, "Edge surface modes in magnetically biased chemically doped graphene strips," *Applied Physics Letters*, Vol. 99, 231902, 2011.
4. Sounas, D. L. and C. Caloz, "Gyrotropy and nonreciprocity of graphene for microwave applications," *IEEE Transactions on Microwave Theory and Techniques*, Vol. 60, 901–914, 2012.
5. Serrano, D. C., J. S. G. Diaz, D. L. Sounas, Y. Hadad, A. A. Melcon, and A. Alù, "Nonreciprocal graphene devices and antennas based on spatiotemporal modulation," *IEEE Antennas and Wireless Propagation Letters*, Vol. 15, 1529–1532, 2016.
6. Zhu, B., G. Ren, Y. Gao, B. Wu, Q. Wang, C. Wan, and S. Jian, "Graphene plasmons isolator based on non-reciprocal coupling," *Optics Express*, Vol. 23, 16071–16083, 2015.
7. Tamagnone, M., C. Moldovan, J. M. Pouirol, A. B. Kuzmenko, A. M. Ionescu, J. R. Mosig, and J. P. Carrier, "Near optimal graphene terahertz non-reciprocal isolator," *Nature Communications*, Vol. 7, 11216(1-6), 2016.
8. Serrano, D. C., J. S. G. Diaz, A. Alù, and A. Á. Melcón, "Electrically and magnetically biased graphene-based cylindrical waveguides: analysis and applications as reconfigurable antennas," *IEEE Transactions on Terahertz Science and Technology*, Vol. 5, 951–960, 2015.
9. Chamanara, N., D. Sounas, and C. Caloz, "Non-reciprocal magnetoplasmon graphene coupler," *Optics Express*, Vol. 21, 11248–11256, 2013.
10. Tamagnone, M., A. Fallahi, J. R. Mosig, and J. P. Carrier, "Fundamental limits and near-optimal design of graphene modulators and non-reciprocal devices," *Nature Photonics*, Vol. 8, 556–563, 2014.
11. Feizi, M., V. Nayyeri, and O. M. Ramahi, "Modeling magnetized graphene in the finite-difference time-domain method using an anisotropic surface boundary condition," *IEEE Transactions on Antennas and Propagation*, Vol. 66, 233–241, 2018.
12. Amanatiadis, S. A., N. V. Kantartzis, T. Ohtani, and Y. Kanai, "Precise modeling of magnetically-biased graphene through a recursive convolutional FDTD method," *IEEE Transactions on Magnetism*, Vol. 54, 233–241, 2018.
13. Wang, X. H., W. Y. Yin, and Z. Chen, "Matrix exponential FDTD modeling of magnetized graphene sheet," *IEEE Antennas and Wireless Propagation Letters*, Vol. 12, 1129–1132, 2013.
14. Cao, Y. S., P. Li, L. J. Jiang, and A. E. Ruehli, "The derived equivalent circuit model for magnetized anisotropic graphene," *IEEE Antennas and Wireless Propagation Letters*, Vol. 65, 948–953, 2017.
15. Shao, Y., J. J. Yang, and M. Huang, "A review of computational electromagnetic methods for graphene modeling," *International Journal of Antennas and Propagation*, Vol. 81, 1–6, 2016.
16. Azizi, M., M. Boussouis, H. Aubert, and H. Baudrand, "A three-dimensional analysis of planar discontinuities by an iterative method," *Microwave and Optical Technology Letters*, Vol. 13, 372–376, 1996.
17. N'gongo, R. S. and H. Baudrand, "A new approach for microstrip active antennas using modal FFT algorithm," *IEEE Antennas and Propagation Society International Symposium*, Vol. 3, 1700–1703, 1999.
18. Gharsallah, A., A. Gharbi, and H. Baudrand, "Efficient analysis of multiport passive circuits using the iterative technique," *Electromagnetics*, Vol. 81, 73–84, 2001.
19. Zairi, H., A. Gharsallah, A. Gharbi, and H. Baudrand, "Analysis of planar circuits using a multigrid iterative method," *IEE Proceedings — Microwaves, Antennas and Propagation*, Vol. 153, 109–162, 2006.

20. Mami, A., H. Zairi, A. Gharsallah, and H. Baudrand, "Analysis of microwave components and circuits using the iterative method," *International Journal of RF and Microwave*, Vol. 81, 404–414, 2004.
21. Aizi, M., H. Aubert, and H. Baudrand, "A new iterative method for scattering problems," *Microwave Conference*, Vol. 1, 255–258, 1995.
22. Houaneb, Z., H. Zairi A. Gharsallah, and H. Baudrand, "Modeling of cylindrical resonators by wave concept iterative process in cylindrical coordinates," *International Journal of Numerical Modelling: Electronic Networks, Devices and Fields*, Vol. 24, 123–131, 2011.
23. Hlali, A., Z. Houaneb, and H. Zairi, "Tunable filter based on hybrid metal-graphene structures over an ultrawide terahertz band using an improved Wave Concept Iterative Process method," *International Journal for Light and Electron Optics*, Vol. 181, 423–431, 2018.
24. Hlali, A., Z. Houaneb, and H. Zairi, "Dual-band reconfigurable graphene-based patch antenna in terahertz band: Design, analysis and modeling using WCIP method," *Progress In Electromagnetics Research C*, Vol. 87, 213–226, 2018.
25. Hlali, A., Z. Houaneb, and H. Zairi, "Effective modeling of magnetized graphene by the wave concept iterative process method using boundary conditions," *Progress In Electromagnetics Research C*, Vol. 89, 121–132, 2019.
26. Hanson, G. W., "Dyadic Green's functions for an anisotropic, non-local model of biased graphene," *IEEE Transactions on Antennas and Propagation*, Vol. 103, 101–109, 2008.
27. Lovat, G., "Equivalent circuit for electromagnetic interaction and transmission through graphene sheets," *IEEE Transactions on Electromagnetic*, Vol. 54, 101–109, 2012.
28. Li, P. and L. J. Jiang, "Modeling of magnetized graphene from microwave to THz range by DGTD with a scalar RBC and an ADE," *IEEE Transactions on Antennas and Propagation*, Vol. 63, 4458–4467, 2015.
29. Guo, Y., T. Zhang, W. Yin, and X. Wang, "Improved hybrid FDTD method for studying tunable graphene frequency-selective surfaces (GFSS) for THz-wave applications," *IEEE Transactions on Terahertz Science and Technology*, Vol. 5, 358–367, 2015.